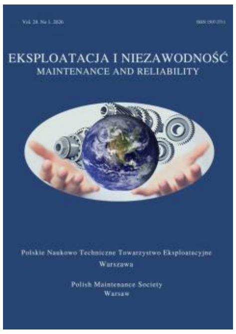

Eksploatacja i Niezawodnosc – Maintenance and Reliability

Volume 28 (2026), Issue 1

journal homepage: http://www.ein.org.pl

Article citation info:
Matijošius J, Žvirblis T, Rimkus A, Stravinskas S, Kilkevičius A, Emissions, reliability and maintenance aspects of a dual-fuel engine (diesel-natural gas) using HVO additive and ANCOVA modeling, Eksploatacja i Niezawodnosc – Maintenance and Reliability 2026: 28(1) http://doi.org/10.17531/ein/208439

Emissions, reliability and maintenance aspects of a dual-fuel engine (diesel-natural gas) using HVO additive and ANCOVA modeling

Indexed by: Web of Science Group

Jonas Matijošius[a,*], Tadas Žvirblis[a], Alfredas Rimkus[b], Saulius Stravinskas[b,c], Artūtas Kilkevičius[a]

[a] Mechanical Science Institute, Vilnius Gediminas Technical University, Lithuania
[b] Department of Automobile Engineering, Vilnius Gediminas Technical University, Lithuania
[c] Department of Transport Engineering, Vilniaus Kolegija Higher Education Institution, Lithuania

Highlights

- Increased NG ratio significantly reduces NOx and smoke emissions.
- HVO pilot fuel shortens ignition delay and lowers injector fouling.
- Dual fuel mode lessens engine thermal load and extends maintenance intervals.
- ANCOVA model predicts major engine parameters with MAPE as low as ~2%.
- Extended intervals and lower component stress improve engine reliability over time.

Abstract

This paper presents an experimental and statistical study of a four-cylinder turbocharged compression ignition (CI) engine operating in dual-fuel mode with natural gas and liquid pilot fuel (diesel or hydrotreated vegetable oil, HVO). The main engine performance indicators (brake power, specific fuel consumption), combustion process parameters (cylinder pressure, heat release rate) and emissions (NO_X, CO_2, smoke) were evaluated, as well as noise and vibration measurements were performed to determine the loading of structural elements. In order to highlight the factors affecting engine reliability and maintenance, the ANCOVA (analysis of covariance) methodology was applied, modeling the influence of load, natural gas fraction and sound pressure. The mean absolute percentage error (MAPE) shows that the model predicts the most important indicators quite accurately under various operating conditions. The developed ANCOVA model not only predicts engine characteristics under various load and fuel mixture conditions, but it also provides insights useful for engine maintenance planning and reliability assurance, especially in long-term or intensive operation.

Keywords
dual-fuel engine, ANCOVA, regression modeling, prognostic models, mean absolute percentage error (MAPE).

1. Introduction

Research on alternative fuels [29] shows that by properly selecting their combinations with conventional fossil fuels [16], it is possible not only to reduce emissions, but also to maintain and improve the reliability and long-term operation of the engine [26]. Dual-fuel technologies, where compressed gas (e.g., natural gas or biomethane) is supplied through the intake manifold, and diesel or other liquid fuel is used as a pilot ignition source, are becoming increasingly popular [12]. This method allows for significant reductions in NO_X and particulate emissions while maintaining sufficient engine power and efficiency [27].

The application of HVO (hydrogenated vegetable oil) as a pilot liquid fuel, partially replacing conventional diesel, is receiving increasing attention. This results in shorter ignition

(*) Corresponding author.
E-mail addresses: J. Matijošius (ORCID: 0000-0001-6006-9470) jonas.matijosius@vilniustech.lt, T. Žvirblis (ORCID: 0000-0002-9368-8726) tadas.zvirblis@vilniustech.lt, A. Rimkus (ORCID: 0000-0001-8995-7180) alfredas.rimkus@vilniustech.lt, S. Stravinskas (ORCID: 0000-0002-5429-4978) saulius.stravinskas@vilniustech.lt, A. Kilkevičius (ORCID: 0000-0002-4039-7300) arturas.kilikevicius@vilniustech.lt ,

delay, cleaner engine combustion, and less polluting of the injector and exhaust system [18, 19]. Using HVO and gaseous fuels in dual-fuel mode also provides operational advantages – lower NO_X and soot emissions allow for shorter maintenance intervals and protect engine components from accelerated wear or deposits [21]. Experimental studies have shown that by properly selecting the amount of HVO, even with an increased proportion of gaseous fuel (e.g., 80% NG by energy), it is possible to maintain similar or even higher engine power, and avoid sudden pressure surges that significantly reduce component life [23]. In addition to emission reduction goals, maintaining operational reliability and minimizing maintenance costs remain key priorities for dual-fuel systems. Acoustic and vibration-based prognostic modeling offers a promising pathway for achieving both objectives simultaneously.

In recent years, examples of machine learning (ML) methods have been rapidly increasing in order to more effectively model [14] and control the combustion processes and emissions of dual-fuel engines [31]. ML algorithms can quickly process large data sets (cylinder pressure, fuel consumption, acoustic signals, emissions) collected during experiments or operations, generating accurate predictions in real time and at the same time helping to understand nonlinear interrelationships between experimental factors [7].

For example, the Boosted Regression Trees (BRT) algorithm can be used to reproduce the performance and emission levels of a dual-fuel engine with high accuracy (correlation coefficient $R^2 \approx 0.995–0.999$) [23]. Compared to conventional artificial neural networks (ANNs), this method often exhibits lower root mean square error (RMSE) and mean absolute percentage error (MAPE), which indicates higher accuracy in reproducing the actual engine performance parameters for various pilot liquid and gaseous fuel compositions. Multi-output regression methods, such as least-squares support vector regression (MLS-SVR), allow a single model to predict several emission components (CH_4, CO, NOx) depending on engine speed, hydrogen content in the intake gas, manifold pressure, and other parameters [9]. This allows for rapid identification of the most appropriate engine control mode to limit the generation of unwanted pollutants [8]. In order to evaluate the impact of various variables—including load, gaseous fuel fraction, and acoustic characteristics—on the combustion process and engine emissions, ML approaches are frequently employed in conjunction with regression analysis and statistical tools like Analysis of Covariance (ANCOVA). ANCOVA models are especially beneficial for dual-fuel engines, as they require an understanding of the interaction between the ratios of liquid pilot and gaseous fuel and the engine load. They allow us to analyze not only the effect of basic components but also their relationships. In another study, where dual-fuel mode used blends of biogas and biodiesel, the Taylor diagram technique also demonstrated that the BRT model nearly identically fits the experimental trends [10].

A novel Taylor's diagram method for comparing dual-fuel engine prediction models demonstrated the advantages of BRT models. To save money, the BRT-based prediction metamodel can mimic future tests. The BTE of biogas-biodiesel was lower than that of diesel. NO_X emissions were lower in dual fuel mode than in fossil diesel mode, however HC and CO emissions were greater. Local fuel generation, on the other hand, saves money on imported gasoline. Thus, addressing energy and environmental challenges with biogas, a low-cost gaseous fuel, is financially feasible. With correlation values ranging from 0.9947 to 0.9997, low Theil's values (less than 0.081), and high Kling-Gupta efficiency (>98%), the proposed BRT model correctly predicted performance and emission parameters. The root mean square error for all output models was 0.0056-0.1154, with a mean absolute percentage error of less than 3%. Under identical operating conditions, the BRT and ANN models were compared. All statistical measurements showed that BRT outperformed ANN. [23]. Multi-output least-squares regression to predict hydrogen-enriched natural gas engine CH_4, CO, and NO_X emissions. The MLS-SVR evaluated these emission parameters based on H_2/fuel ratio, engine speed, manifold absolute pressure, surplus air ratio, and ignition duration. The study's key findings are below. MLS-SVR allowed MIMO simulation of HENGE emission properties. NO_X and CH_4 emission are mainly affected by surplus air ratio, while CO emission is most affected by manifold absolute pressure [9]. The suggested modeling and ABC (Artificial Bees Colony Algorithm) parameter optimization approach involves two steps. First, polynomial regression is used to model and optimize SI (Spark ignition) engines output performance using testing data. Compare R^2 and RMSE. The proposed polynomial regression integrated with the ABC optimization technique showed excellent predictive reliability. When using AC10 (Gasoline fuel and 10 % of acetone by volume fuel mixture) instead of pure diesel, polynomial regression and ABC optimization would increase SI engine BT and BTE (Brake thermal efficiency) by 6.33% and 10.59%, respectively [2].

In addition to targeted modeling of emissions and combustion parameters, ML methods are widely used in engine diagnostics: acoustic and vibration signals processed by neural networks or statistical classifiers allow for real-time detection of atypical operating modes (misfire, detonation, excess temperature), thereby increasing operational reliability and predicting the need for maintenance [24, 30]. For example, by creating a neural network that captures anomalies in the dynamics of combustion pressure changes, it is possible to determine that the pilot injector or gas injection system is operating unevenly before a major failure occurs. This is extremely important in order to respond in a timely manner to increased NO_X or vibration levels [28].

In summary, numerical models based on machine learning principles already allow:

- Quickly and accurately predict dual-fuel engine emissions (NO_X, smoke, etc.) and operating parameters (cylinder pressure, combustion duration, heat release rate) [3, 11, 20].
- Statistically assess the significance of several parameters (load, fuel composition, acoustic indicators) and their interaction, describing complex nonlinear relationships [32].
- Diagnose engine condition and predict maintenance needs based on sensor data, thus extending operational reliability [17].
- Optimize the use of dual-fuel technology in real time, reducing the cost of experimental testing and increasing applicability to various engine types or fuel mixtures [22].

Further development of these methods will contribute to even greater efficiency of dual-fuel systems and will help create the prerequisites for the widespread application of sustainable fuels (e.g. HVO, biomethane, biogas), making maximum use of the possibilities provided by new generation algorithms for controlling combustion processes [5].

A higher proportion of gaseous fuel (up to ~60–80% of energy) reduces soot, NO_X emissions and thermal loading of the cylinder walls [18]. This means that fewer deposits (carbons, sulfur compounds) are formed, injectors and distributors become clogged more slowly, and the load on the exhaust gas recirculation (EGR) system decreases [25]. This change extends the periods between maintenance procedures (e.g., cleaning injectors, changing oil due to soot). Lower maximum temperatures in the combustion chamber also reduce thermal fatigue of parts, so the engine runs longer without major repairs [6].

However, the dual-fuel mode itself requires additional maintenance of the gas injection (or dosing) system itself, pressure regulation and condensate collection. However, ML models already offer the ability to predict malfunctions in these systems – for example, uneven gas flow or inaccurate pilot nozzle operation can be determined by increased emissions or anomalous vibration spectra [13]. This allows for real-time identification of possible operational deviations before they turn into a major failure.

1. The combination of gas and liquid pilot in the engine combustion chamber helps reduce NO_X and particulate matter (smoke) levels, while maintaining similar or even higher efficiency. As a result, the accumulation of deposits is reduced, engine parts are less stressed, which directly extends the service life of components [1, 15].
2. HVO fuel (as an alternative to diesel for pilot injection) has a lower sulfur and aromatic content, therefore it pollutes the injectors and exhaust system less, increasing the reliability of the engine during long-term use [18].
3. Machine learning methods (BRT, ANCOVA, neural networks) allow for effective prediction of engine combustion and emission indicators, determination of optimal operating conditions and timely identification of possible signs of failure. This means the ability to adapt engine control in real time and thus reduce operating costs and risks [23].
4. Operational reliability depends on many factors – combustion dynamics, fuel quality, engine load, vibrations, and the dual-fuel mode requires more

precisely coordinated control algorithms. However, by applying ML models, it is possible to identify the most important risk factors, respond in time to atypical combustion or vibration signals, and thus reduce repair intervals [28].

Thus, current trends show that the dual-fuel (liquid pilot + gaseous fuel) concept, enhanced by artificial intelligence analysis tools, is a sustainable and promising direction for reducing pollutant emissions, ensuring stable engine operation, and extending service life. The integration of ML methods in dual-fuel systems provides the opportunity not only to predict real operating parameters, but also to timely identify future malfunctions or changed operating conditions, thereby reducing repair and downtime costs.

2. Methodology and Data Description

2.1. Conditions of the Tests and Engine Outcome Parameters

Dual fuel compression-ignition (CI) engine with load bench was used in experimental studies (Fig. 1). It was four-cylinder high-speed turbocharged engine with direct liquid fuel injection system (Table 1). The CI engine was additionally equipped with a gaseous fuel supply system (Elpigaz-Degamix) ensuring precise mass-controlled gas injection into the intake air before the turbocharger.

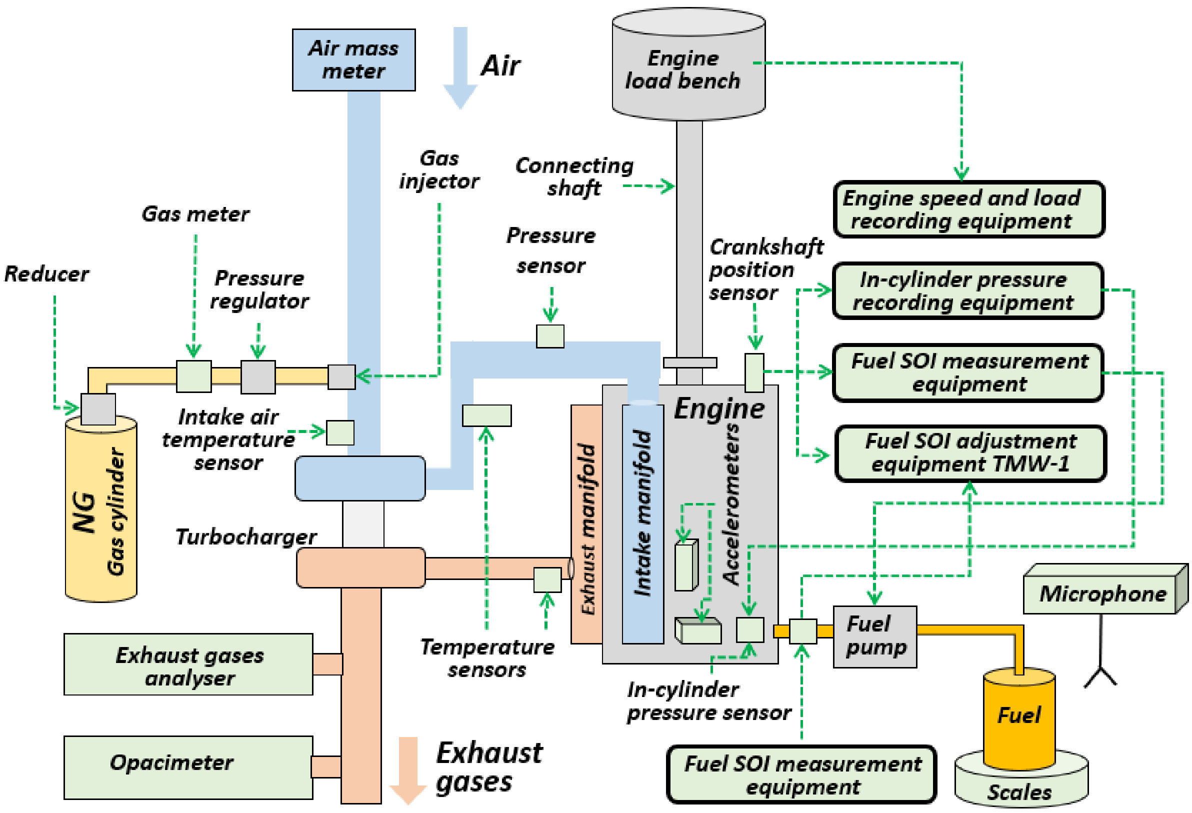

Figure 1. Scheme of experimental studies.

Engine load torque M_B (measurement error ± 1.23 Nm) and crankshaft speed n (rpm.) were regulated with a load bench KI-5543. An electronic scale SK-5000 (measurement error: 0.5%) and a chronometer were used to measure the consumption of liquid fuel mass per hour B_f (kg/h). Natural gas consumption was measured with an RHM 015 type mass flow meter (measurement error: ± 0.1%). The intake air mass was measured with a Bosch HFM 5 (measurement error: 2%) air mass meter. The in-cylinder pressure was measured using an AVL GH13P sensor installed in a place of the glow plug (sensitivity of piezoelectric sensor: 15.84 ± 0.09 pC/bar) and recorded using LabView Real software and an AVL DiTEST DPM 800 oscilloscope (signal ratio: 1 mV/pC, input range: 6000 pC). An A58M-F photoelectric encoder was used to determine the position of the crankshaft rotation angle (CA) (signal repeatability: 0.176° for the CA). Pressure in the engine intake manifold was measured with a Delta OHM HD 2304.0 device (measurement error: ± 0.0002 MPa). Intake and exhaust temperatures were measured using K-type thermocouples (measurement error: ± 1.5 °C). The composition of chemical elements in the exhaust gas was measured using an AVL DiCom 4000 exhaust gas analyser/opacimeter (Table 2).

Table 1. The specifications of the tested CI dual fuel engine.

Indicator	Dimension	Value
Engine displacement V_H	cm^3	1986
Cylinders	arrangement	Four, in-line
Valve control system	-	OHC
Compression ratio ε	-	19.5
Bore D	mm	79.5
Stroke S	mm	95.5
Max. Power P	kW	66 (4000 rpm.)
Max. Torque M	Nm	182 (2000–2500 rpm.)
Injectors opening pressure p_i	bar	190–200
Fuel injection system	-	Distributor injection pump

Table 2. Specifications of the exhaust gas analyser.

Measured indicator	Dimension	Measurement range	Accuracy
CO_2	% (vol.)	0–20	0.1
HC	ppm (vol.)	0–20000	1
NO_X	ppm (vol.)	0–5000	1
O_2	% (vol.)	0–25	0.01
λ	-	0–1.0	0.001
Smoke absorption coefficient	m^{-1}	0–99.99	0.01
Engine speed	rpm	250–9990	10

Engine speed (n = 2000 rpm) was constant during all tests, but there were three different engine loads: M_B = 45, 60 and 90 Nm (corresponding brake mean effective pressure (*BMEP*): 0.3, 0.4 and 0.6 MPa). Start of liquid fuel injection (SOI) was fixed at 6° CA before top dead centre (BTDC), as the standard engine control unit begins to adjust SOI do to the addition of gaseous fuel. Reason of this is lower mass of liquid fuel required to maintain the specified torque. Received data with fixed constant start of injection moment allows the combustion process of different fuels to be compared. Engine speed and loads were selected to correspond real driving conditions on the highway or stationary engine working as a generator. Tests were performed without using EGR system.

Main combustion parameters, such as start of combustion (SOC), combustion duration (CD), combustion intensity index – Wiebe equation factor m, rate of heat release (ROHR), in-cylinder pressure rise, in-cylinder pressure and temperature, were set using AVL BOOST sub-software BURN. The parameters measured in experimental research (fuel consumption, air flow, cylinder pressure, boost pressure, etc.) were used to determine these parameters.

2.2. Type of Fuel

Conventional diesel or hydrotreated vegetable oil biodiesel (HVO) was used as a pilot fuel to ignite the gas in the cylinder. Natural gas was supplied to the intake manifold. Table 3 shows dual fuel composition, marking and lower heating (energy) values (LHVs).

Table 3. Tested fuels and their labels.

Fuel (% of energy) Liquid fuel	Gaseous fuel	Label	*LHV*, MJ/kg
Conventional diesel fuel and natural gas			
100%	0%	D100	42.82
60%	40%	D60+NG40	45.45
40%	60%	D40+NG60	46.92
20%	80%	D20+NG80	48.49
Hydrotreated vegetable oil and natural gas			
100%	0%	HVO100	43.63
60%	40%	HVO60+NG40	46.04

40%	60%	HVO40+NG60	47.25
20%	80%	HVO20+NG80	48.83

2.3. Vibration and sound pressure of the engine

Vibrations produced by internal combustion (IC) engines rely on disbalanced return motion and rotating components, cyclical gas pressure variation, dynamic excitation forces from engine rotating elements, and structural characteristics of the engine mounting system. General views of engine vibration and sound pressure measurement points are presented in Fig. 2. In the low frequency band, the engine mounting structure's stiffness and damping must be high; in the high frequency range, they must be low. Engine vibrations must be reduced by correct engine mounting. Occasionally, it is required to use mounting components with suitable qualities at the contact point between the engine and frame. Often, several kinds of vibration insulation material are employed to lower engine-to-mounting structure force transmission.

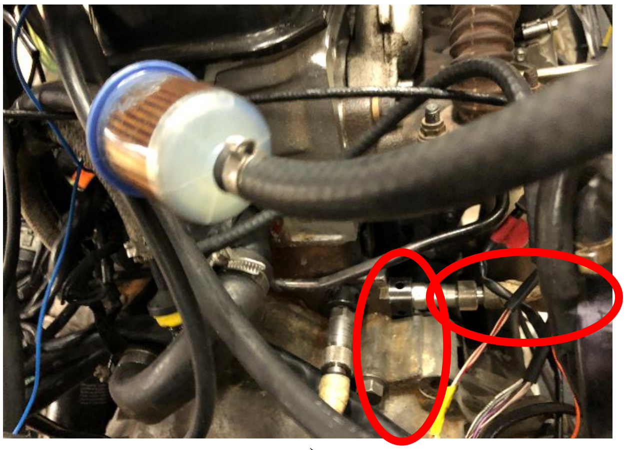

a) b)

Figure 2. Vibration and sound pressure measuring points: (a) an overview of the engine under examination and vibration measurement points; (b) a microphone for sound pressure measurement.

Noise of the surrounding surroundings and vibrations did not influence room measurements during experimental engine tests. The test room walls had a soundproof double-glazed glass for looking inside the engine test chamber from the operator's room, an acoustic door, and an acoustic lining composed of sound-insulating material.

Using a Gras 46AE free-field microphone (range: 3.15–20,000 Hz; dynamic range: 17–148 dB; sensitivity: 50 mV/Pa.) assessed the compression of an ignition engine's sound pressure. Engine block vibrations in longitudinal and transverse directions were measured using Bruel and Kjaer 8341 CCLD accelerometers (frequency range: 0.3–10,000 Hz; sensitivity: 0.01 V/ms^{-2}). Noise and vibration data were gathered using the Bruel and Kjaer Machine Diagnostic Toolbox Type 9727 (comprises 5-channel PULSE data collecting equipment Type 3560-B). Bruel and Kjaer program processed collected vibration and sound pressure data. Sound pressure and vibration data were collected from the engine block at a frequency of 3.2 kHz (for vibration) and 20.0 kHz (for sound pressure) for all tested fuels and engine loads.

Although a free-field microphone was used for sound pressure measurements, the focus was on relative signal features (RMS and spectral content), and the test cell environment allowed for sufficient control of reflections. Future studies will consider pressure-field microphones to enhance near-field accuracy.

2.4. Statistical Analysis

Multivariate linear regression models for predictions of maximum in-cylinder pressure, NO_X, smoke, exhaust gas temperature, SOC, CD, m, and RORH were build. Power, gas ratio, sound pressure, and vertical vibrations were selected as independent prognostic variables. Whole experiment data was divided in to two sets: training and test sets. Training and test sets consisted of experimental data when pure diesel and HVO was used, respectively. Multivariate regression models were based on analysis of covariance (ANCOVA) model [2, 4]. Model for training data set was defined as:

$$Y^{E,D} = \alpha^D + \beta^D P^D + \gamma^D R^D + \delta^D S^D + \theta^D V^D + \varepsilon,$$

where $Y^{E,D}$ – engine outcome parameter (dependent variable), E – type of engine outcome parameter, D – indicator of experiment when pure diesel was used, P^D – engine power, R^D – gas ratio, S^D – sound pressure RMS, V^D – vertical vibrations RMS, α^D – regression intercept value, β^D – regression parameter for engine power, γ^D – regression parameter for gas ratio, δ^D – regression parameter for sound pressure, and θ^D – regression parameter for vertical vibrations, ε – random error.

After parameter estimation new prognostic model for test set was build:

$$Y^{E,HVO} = \alpha^D + \beta^D P^{HVO} + \gamma^D R^{HVO} + \delta^D S^{HVO} + \theta^D V^{HVO},$$

where $Y^{E,HVO}$ – engine outcome parameter (dependent variable), E – type of engine outcome parameter, HVO – indicator of experiment when HVO was used, P^{HVO} – engine power, R^{HVO} – gas ratio, S^{HVO} – sound pressure RMS, V^{HVO} – vertical vibrations RMS, α^D – regression intercept value, β^D – regression parameter for engine power, γ^D – regression parameter for gas ratio, δ^D – regression parameter for sound pressure, and θ^D – regression parameter for vertical vibrations.

Sound pressure and vertical vibrations signals were aggregated with root mean square (RMS) estimate for each experiment:

$$RMS = \sqrt{\frac{1}{N}\sum_{i=1}^{N} x_i^2},$$

where N – sample size, x – value of sound pressure signal.

Accuracy between prognostic model and real data was evaluated using mean absolute percentage error (MAPE):

$$MAPE = \frac{1}{N}\sum_{i=1}^{N}\left|\frac{Y_i^{E,HVO} - \hat{Y}_i^{E,HVO}}{Y_i^{E,HVO}}\right|,$$

where $Y_i^{E,HVO}$ – observed engine outcome parameter value for i^{th} experiment, $\hat{Y}_i^{E,HVO}$ – prognostic engine outcome parameter value for i^{th} experiment, E – type of engine outcome parameter, HVO – indicator of experiment when HVO was used.

3. Results and Discussion

3.1. Sound Pressure of the Engine

The diagrams in Fig. 3 show the time and frequency domain variations of the sound pressure of different fuel mixtures (HVO100NG00, HVO60NG40, HVO40NG60) at a load of 60 Nm. First, when using only HVO (HVO100NG00), the combustion is characterized by a somewhat faster SOC and a sharper pressure rise, since there is no diluted gas component that would make the combustion process more uniform. In this case, larger instantaneous sound peak jumps are visible in the time domain, indicating more intense combustion dynamics. In the frequency domain, this influence of combustion sharpness is manifested by more pronounced peaks in the mid- and higher-frequency range, often corresponding to engine structural resonances or knock-like phenomena.

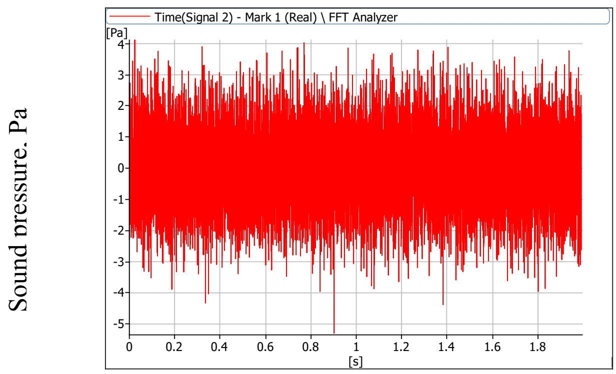

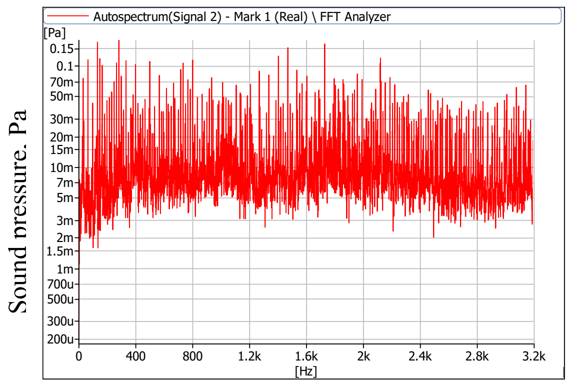

a)

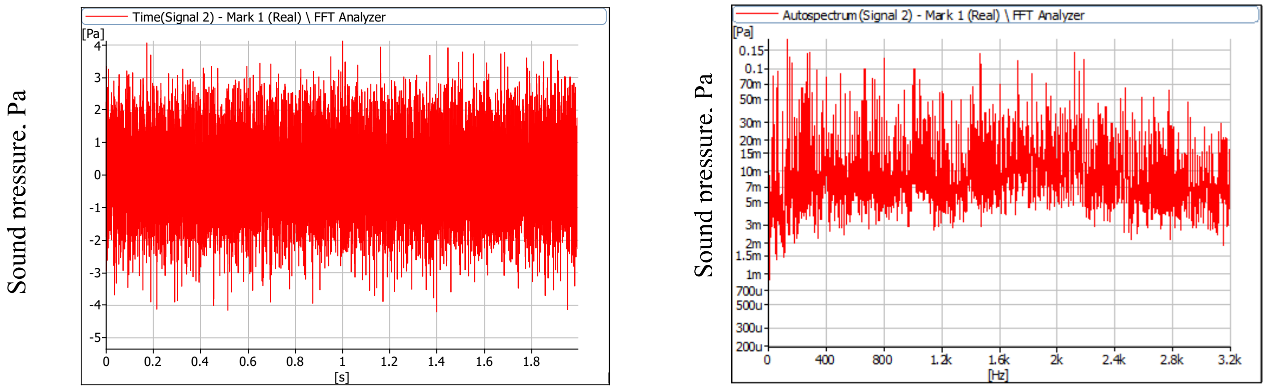

b)

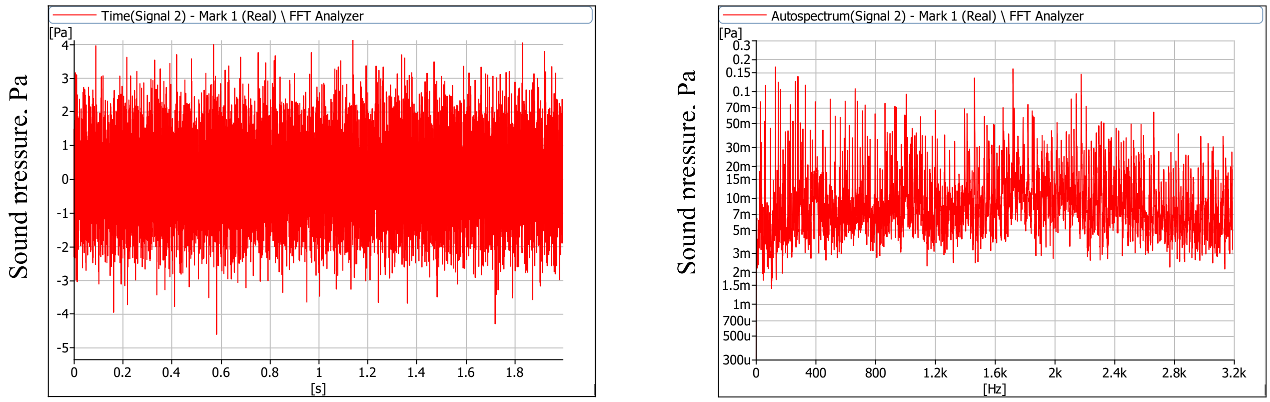

c)

Figure 3. Typical results of measurement of sound pressure (a – HVO100NG00; b – HVO60NG40; c – HVO40NG60) under 60 Nm load.

On the other hand, when switching to the mixed variants HVO60NG40 and HVO40NG60, the pilot combustion still takes place partly with liquid fuel (HVO), but a significant part of the energy is provided by natural gas entering the cylinder during the intake. Such a mixture is created more restrained during combustion, because the gas ignites more slowly and is more evenly distributed in the combustion chamber. As a result, the pressure rise becomes less abrupt, the amplitude of instantaneous jumps decreases. In the time-domain graphs, the total sound level may remain close to the pure HVO mode, but the frequency domain (autospectral) analysis reveals that the acoustic energy is distributed in a wider frequency band, therefore the sharpest peak intervals weaken. This indicates that the gas part acts as a shock absorber that softens the combustion pulses.

From a physical point of view, an intense increase in sound pressure is associated with a sharp change in pressure at the beginning of combustion, when the accumulated fraction of combustible vapors burns out in a short time. In the case of pure HVO, this fraction can ignite very quickly, generating a larger acoustic response. When natural gas is added, the combustion front is stretched: the pressure rises in a flatter curve, while the probability of sudden structural excitation decreases. As a result, engine design resonances and combustion shocks, especially in the mid-frequency range, cause smaller amplitudes. From a practical point of view, such a trend means that increasing the NG fraction reduces the engine noise at sharper frequencies, but the total RMS value in the time domain may remain similar, since the total amount of thermal energy released is essentially unchanged.

The final conclusion would be that the HVO100NG00 variant leads to more intense sound pressure dynamics due to the more static nature of combustion, while in the case of HVO60NG40 and HVO40NG60, the combustion energy is naturally distributed between the liquid and gaseous fuels, reducing the most pronounced frequency peaks and softening the impulse noise component. This expresses a strong cause-and-effect relationship between fuel composition (higher or lower gas content) and the acoustic response of the engine (noise and vibration levels).

3.2. Descriptive Statistics of Exhausted Emission Parameters

Descriptive analysis was performed for all engine outcome parameters, vibrations RMS, and sound pressure RMS in fuel type groups. The mean values of majority of engine outcome parameters and sound pressure RMS did not differ between diesel and HVO groups (Table 1). Only ignition delay vertical vibrations was found to be statistically significantly higher in diesel groups ($p = 0.010$ and 0.004, respectively).

Tables 1 and 2 show how the engine performance and emission indicators change when using different liquid fuels (diesel and HVO) and various natural gas (NG) fractions. First, comparing the use of pure diesel and HVO without a gas additive, it is noticeable that the mean (SD) of the maximum combustion pressure (77.4 (8.66) MPa and 76.5 (9.30) MPa), NO_X (346 (224) and 323 (211) ppm) and smoke (3.6 (0.82) and 3.3 (0.84) m^{-1}) do not differ significantly. Peak pressure and NO_X decrease due to slower NG combustion at lower combustion temperatures, but smoke decreases due to the lower carbon/hydrogen ratio in the natural gas and the longer combustion process. However, two parameters stand out more: start of combustion (SOC) and vertical engine vibrations. In the case of HVO, the degree of SOC timing is statistically significantly lower than that of diesel, and the vibrations in the vertical axis are higher. This indicates that HVO, having different aspects of combustion chemistry, causes a slightly faster combustion initiation stage, but due to different pressure growth dynamics, it excites the engine block more in the vertical direction.

Secondly, when introducing different amounts of natural gas (0%, 40%, 60% and 80% of energy from NG), a clear trend emerges: as the NG fraction increases, the maximum pressure decreases (from ~80 to ~72 MPa), NO_X (from ~508 to ~209 ppm) and smoke (from ~4.1 to ~2.3 m^{-1}) decrease significantly. Thus, partial gas combustion smoothes the nature of the pressure variation and reduces the formation of nitrogen oxides and particulate matter (soot). It is also seen that the exhaust gas temperature increases slightly with increasing NG content (from ~349 to ~368 °C), and ROHR (heat release rate) decreases slightly – combustion becomes less impulsive, because the amount of liquid fuel decreases, and more evenly distributed gases stretch the combustion process. In other words, due to the slower combustion of natural gas, the energy of the exhaust gases tends to increase as the share of NG energy increases.

Both the SOC timing, combustion duration (CD) and sound pressure RMS values differ less significantly, but vibrations (especially vertical) with a higher NG content noticeably decrease (from ~55 to ~48 RMS). This correlation allows us to understand that increasing the natural gas energy fraction reduces sudden pressure surges at the beginning of combustion, therefore, the engine block is subjected to less impulsive mechanical impact. However, overall sound pressure RMS can remain quite similar, since the engine still generates similar total heat and sound energy, only the nature of the distribution of this energy changes.

Table 1. Descriptive statistics of engine outcome parameters, sound pressure, and vibration data in fuel groups.

Parameter	Total Mean (SD)	Pure diesel Mean (SD)	HVOMean (SD)	p-value
Max in-cylinder pressure, MPa	77.0 (8.80)	77.4 (8.66)	76.5 (9.30)	0.796
NO_X, ppm	334.6 (213.20)	346.2 (224.25)	323.0 (210.86)	0.797
Smoke, m^{-1}	3.4 (0.83)	3.6 (0.82)	3.3 (0.84)	0.324
Exhaust gas temperature, °C	358.9 (45.18)	359.9 (45.89)	357.8 (46.48)	0.913
RORH, J/°CA	34.3 (10.23)	35.9 (9.21)	32.8 (11.34)	0.473
SOC, °CA BTDC	3.9 (0.66)	4.2 (0.72)	3.5 (0.40)	0.010
CD, °CA	50.6 (7.27)	51.9 (8.05)	49.3 (6.49)	0.399
m	0.99 (0.246)	0.92 (0.272)	1.06 (0.205)	0.174
Sound pressure RMS, m/s^2	1.12 (0.089)	1.13 (0.088)	1.10 (0.091)	0.397
Vertical vibrations RMS, m/s^2	52.6 (7.03)	48.7 (5.70)	56.5 (6.18)	0.004
Horizontal vibrations RMS, m/s^2	23.96 (1.20)	23.9 (1.20)	24.0 (1.24)	0.737

Table 2. Descriptive statistics of engine outcome parameters, sound pressure, and vibration data in gas energy ratio groups.

Parameter	Gas energy ratio, %			
	0 Mean (SD)	40 Mean (SD)	60 Mean (SD)	80 Mean (SD)
Max in-cylinder pressure, MPa	80.4 (6.62)	78.8 (8.55)	76.9 (9.72)	71.7 (38.61)
NO_X, ppm	508.5 (165.71)	331.3 (218.80)	289.8 (207.82)	208.7 (123.83)
Smoke, m^{-1}	4.1 (0.44)	4.1 (0.36)	3.3 (0.38)	2.3 (1.90)
Exhaust gas temperature, °C	349.0 (49.93)	357.8 (46.83)	360.8 (51.18)	367.8 (167.97)
RORH, J/°CA	35.3 (5.96)	34.9 (7.88)	34.9 (13.08)	32.3 (14.45)
SOC, °CA BTDC	4.0 (0.77)	3.8 (0.68)	3.8 (0.68)	3.8 (1.74)
CD, °CA	52.0 (2.84)	51.0 (4.49)	49.0 (9.01)	50.4 (24.87)
m	0.77 (0.069)	0.90 (0.133)	1.11 (0.231)	1.17 (0.446)
Sound pressure RMS, m/s^2	1.12 (0.090)	1.14 (0.053)	1.13 (0.090)	1.08 (0.578)
Vertical vibrations RMS, m/s^2	54.5 (6.93)	55.8 (6.38)	52.4 (6.65)	47.8 (7.10)
Horizontal vibrations RMS, m/s^2	24.8 (1.57)	24.0 (1.34)	23.8 (0.58)	23.3 (0.83)

In summary, simply changing the liquid fuel from diesel to HVO significantly affects only the ignition duration and the level of vertical vibration, while increasing the natural gas energy fraction radically reduces NO_X and smoke, smoothes out maximum pressure in-cylinder and vibrations. Such results highlight that the inclusion of NG in the combustion process provides ecological and dynamic benefits, allowing for the maintenance of similar engine power with lower emissions and smoother combustion.

These combustion and emission trends are also relevant from a mechanical reliability perspective. Lower peak in-cylinder pressures and smoother pressure rise curves suggest reduced mechanical loading of engine components, while decreased vibration RMS values indicate diminished structural stress. Together, these factors point to a potentially longer service life of engine parts and extended maintenance intervals under high NG ratio operation.

3.3. Prognostic Model Building

For the prognostic model building experimental data was divided in to two sets: training and test. Training data set was used for estimation of prognostic model parameters while test sets was used for final model application and accuracy evaluation. Multivariable ANCOVA model was trained using experimental data when pure diesel was used. Parameter estimates are shown in Table 3.

The parameters of the trained multivariate ANCOVA model are presented in Table 3. The model parameters indicate how many units of measurement the dependent variable increases when the independent variable increases by one unit or moves to another category.

Table 3. Model parameters estimation using training set.

Parameters		Max in-cylinder pressure, MPa	NO_X, ppm	Smoke, m^{-1}	Exhaust gas temperature, °C	RORH, J/°CA	SOC,°CA BTDC	CD, °CA	m
Intercept		82.31	868.42	3.63	558.42	2.61	4.90	120.27	-0.97
Gas energy ratio, %	0	9.19	326.38	1.91	-14.47	0.83	0.16	5.28	-0.53
	40	7.39	152.18	1.88	-2.42	-1.36	-0.03	8.52	-0.56
	60	6.07	119.35	1.06	0.48	3.06	0.09	3.51	-0.24
	80	0	0	0	0	0	0	0	0
Engine power, kW	45	-17.93	-481.51	-0.59	-123.28	-12.08	1.37	3.05	-0.08
	60	-13.49	-351.06	-0.31	-72.04	-20.70	0.28	13.38	-0.42
	90	0	0	0	0	0	0	0	0
Sound pressure RMS, m/s^2		-7.68	-353.38	-0.74	-105.03	-7.98	-2.24	-34.77	1.04
Vertical vibrations RMS, m/s^2		0.18	0.14	-0.02	-0.21	1.08	0.03	-0.79	0.02
R^2		98.4	99.0	99.5	99.7	90.6	98.7	72.0	90.8
p-value		0.002	<0.001	<0.001	<0.001	0.059	<0.001	0.372	0.047

The Table 3 presents the coefficients of ANCOVA training model estimated from the experimental data, when the pilot fuel was pure diesel, and the output characteristics evaluated ranged from maximum in-cylinder pressure to the combustion intensity index m. The intercept value for all indicators (e.g., 82.31 MPa for max. in-cylinder pressure, 868 ppm NO_X, 3.63 m^{-1} for smoke, etc.) reflects the base position of the model, relative to which the coefficients of the effects of other variables (gas ratio, engine power, sound pressure and vibrations) are evaluated. The effect of the gas ratio is decomposed into four levels – 0%, 40%, 60% and 80%, where 80% NG is considered the reference point (value in the table = 0). The maximum pressure line shows that when the gas fraction is 0% (i.e. diesel fuel only), the pressure increases by +9.19 MPa compared to the base 80% NG energy ratio. The same principle applies to 40% and 60% NG energy ratio (+7.39 and +6.07 MPa). These positive numbers show that as the gas content decreases (as the liquid fuel fraction increases), the combustion becomes more intense, therefore the pressure peak increases. The same trend is confirmed by the NO_X line, where 0% NG energy ratio leads to as much as +326 ppm more NO_X than the base 80% NG, while at 40% and 60% NG, this excess amounts to +152 ppm and +119 ppm, respectively. Thus, a higher natural gas fraction significantly reduces the formation of nitrogen oxides. A similar result is observed in terms of smoke level: 0% NG increases smoke level by +1.91 Pa, while at 60% NG it is only +1.06 Pa above the base, which indicates that a higher proportion of gas reduces soot formation. The exhaust gas temperature changes slightly differently. At 0% NG, the temperature decreases by –14.47°C, but as it approaches 60% NG, the effect becomes even slightly positive (+0.48°C), indicating that the combustion process may take place in a different mode here, and the total heat is released more evenly. RORH (heat release rate) does not yet have a unidirectional trend: at 0% NG it increases by +0.83, at 40% NG by –1.36, and at 60% NG it rises by +3.06. This makes it clear that heat release depends not only on the gas fraction, but also on other combustion parameters occurring at the same time. The effect of engine load (Engine power) is compared from 45 kW and 60 kW relative to a 90 kW base. When the load is reduced to 45 kW, a significant drop in peak pressure (–17.93 MPa) and NO_X (–482ppm) is observed. In addition, a lower exhaust gas temperature (–123.28°C) and a lower RORH (–12.08) are obtained. This means that when the engine is operating at lower power, the combustion process is less intense, so the pressure and temperature peaks are smaller, and the NO_X concentration is also significantly reduced. It is noticeable that the combustion duration (CD) increases slightly (e.g. +3.05°CA degrees at 45 kW and +13.38 at 60 kW), which indicates that combustion may be slower at lower loads. It is worth paying attention to the SOC timing: a lower load (45 kW) in the model is associated with a slight (+1.37° CA) increase in this parameter, which may indicate a slightly different phase of combustion initiation. Analyzing the last two rows – sound pressure RMS (Sound pressure RMS) and vertical vibrations RMS (Vertical vibrations RMS) – it is possible to assess how acoustic and dynamic phenomena are related to the combustion process. For example, with an increase in the sound pressure RMS value, the maximum in-cylinder pressure in the model changes by –7.68 MPa from the base, NO_X decreases by as much as –353 ppm, and RORH – by –7.98. Such coefficients indicate that a more intense acoustic environment (higher RMS) is inherently associated with certain changes in combustion. And the RMS of vertical vibrations, for example +0.18 MPa at maximum pressure and +0.14 ppm at NO_X, show that increasing block vibrations correlate with somewhat higher pressure and NO_X formation. However, these are statistical relationships that do not necessarily directly define what causes what, but it is obvious that combustion and acoustic-dynamic engine properties are closely related. In summary, high R^2 values (from ~90% to ~99.7%) confirm that the variables included in the ANCOVA model (gas fraction, engine load, sound pressure and vibration RMS) explain most of the differences between the experimentally measured combustion and emission indicators. Such a model allows us to quantitatively assess how a decreasing NG fraction or lower power is directly related to increased maximum in-cylinder pressure, NO_X or smoke; and also shows how the acoustic and vibrational state of the engine is related to the combustion process parameters. At the same time, this confirms that the increasing proportion of natural gas (especially towards 80% of the energy ratio) remains effective in reducing the pressure peak and NO_X formation, and when the load is reduced, the processes become less intense, but the combustion stretches out over a longer angular interval.

After parameter estimation final prognostic models was validated on test set. Prognostic and real engine parameter trends are shown in Figs. 4–6.

Figure 4a shows the maximum in-cylinder pressure (MPa) in twelve experiments with varying engine load and natural gas (NG) fraction. The blue curve shows the actual (observed) values, while the red curve shows the values predicted by the ANCOVA test model. The overall data development clearly confirms that the pressure decreases with increasing NG fraction, and increases with increasing engine load. In the lower load range (runs 1–4), when the NG energy ratio increases from 0% to 80%, a close, albeit slightly overestimated, agreement between the experimental and predicted results is observed; for example, in run 1 the model shows a slightly higher in-cylinder pressure than the experimentally recorded pressure. In the middle load range (runs 5–8) the differences between the actual and numerical values decrease, indicating a more even match. In the maximum load regime (9–12 tests), the predictions again tend to slightly overestimate or, in some cases, underestimate the real in-cylinder pressure by several MPa, but overall the red and blue curves move along the same trajectory. This means that the model adequately captures the pressure variation trends and the relative deviation caused by changes in the NG energy ratio and the increase in load. Even in cases where the predicted pressure differs slightly from the observer, the difference usually does not exceed 3–4 MPa, which indicates that the model developed on the basis of ANCOVA generally correctly reflects the influence of the two fuels (diesel and natural gas) on the maximum in-cylinder pressure at different loads.

Figure 4b shows the exhaust gas temperature (°C) over twelve tests (blue curve) and the same temperature values predicted by the ANCOVA model (red curve). It is immediately apparent that the experimental data show a consistent temperature increase, from around 300°C (at lower load and higher natural gas fraction) to over 420°C as the engine power increases and the fuel composition changes. The model output curve also presents a gradual increase, usually slightly exceeding the actual measured temperature in the first tests (e.g., 299°C observed in test 1, and 303.2°C predicted), but the differences remain small and systematically decrease in the higher load zone. For example, in tests 5–8 the observed temperature increases from 336°C to 349°C, while the model shows 337.8–363.6°C. Although there is a 14°C difference in run 8 (observed 349°C, predicted 363.6°C), the overall increasing trend of both curves coincides. Finally, in the peak load section (runs 9–12), when the temperature actually approaches 420 °C, the model also predicts it in a similar range (~409–420°C), actually coinciding very closely with the observed curve values. In general, both experimental and model data show that when moving to higher engine power and decreasing the proportion of natural gas, the temperature increases steadily. Although the ANCOVA model results in the first runs exceed the actual values by an average of 5–10°C, in the later runs (especially 9–12) the prediction approaches almost perfectly. Such dynamics confirm that the model successfully conveys the fundamental regularity of heat variation, arising both from the intensification of combustion processes with increasing load and from the influence of fuel composition on the thermal conditions of the engine.

Figure 5a shows the NO_X emission levels (blue curve) for twelve experimental runs and the ANCOVA model predictions for the same parameter (red curve). The data are divided into three main load levels (runs 1–4, 5–8 and 9–12), each with a different natural gas energy ratio. In all cases, NO_X emissions clearly decrease with increasing NG fraction in the mixture, and the ANCOVA model curve follows the same decreasing trend, although at some points it tends to overestimate the observed values. In the first interval (runs 1–4), NO_X drops from around 350 ppm to 60 ppm, when the NG energy ratio reaches 80%. The model predicts slightly higher NO_X levels in this range (e.g. 351 vs. 367), but it reflects the general downward trend well. In the second interval (5–8 tests), at medium load, a fairly large difference is seen between 430 ppm (low NG content) and 120 ppm (80% NG); the model also shows higher predictions, but the direction of change clearly coincides. In the third interval (9–12 tests), where the load is highest, the actual NO_X values increase to 700 ppm, while the model – to almost 790 ppm, but again with decreasing NG content, the same tendency for emissions to decrease is detected. In general, although the ANCOVA model tends to slightly overestimate the NO_X concentration at most points, its accumulated deviation is relatively small, especially considering that NO_X values reach several hundred or even up to 700–800 ppm. The main conclusion remains clear: NO_X emissions decrease significantly with increasing natural gas content, and the model adequately reflects not only this trend, but also the deviations of individual tests and the influence of load.

Figure 5b shows the variation of smoke in different test cases (blue curve) and the corresponding ANCOVA model predictions (red curve). As in the other indicators, each block of four tests (1–4, 5–8, 9–12) reflects a constant engine load, but a changing natural gas energy ratio from 0% to 80%. In all three groups of blocks, a very clear decrease in smoke with increasing NG proportion is observed. For example, at the end of the first block (test No. 4) smoke decreases to 1.9 m^{-1}, while in the initial test (No. 1) it was 3.4 m^{-1}. The same drop is shown by the model predictions – from 4.1 to 2.3, only the model records a higher smoke value on average (typically 0.2–0.6 m^{-1} above the observed one). In the second block (runs 5–8), where the load increases, the smoke also decreases from almost 3.7 to about 2.0, while the model curve moves from 4.2 to 2.4. Here again, it is clear that both the observed and predicted values point in the same direction, but the ANCOVA results tend to overestimate the actual smoke. In the third block (runs 9–12), where the load is even higher, the total smoke value starts at 4.4 m^{-1} (low NG fraction) and drops to 2.4 m^{-1} (80% NG), while the model calculates 4.6 → 2.6 m^{-1}. In summary, although the model values remain somewhat higher than the experimental ones in most runs, the overall decreasing trend is completely consistent: with increasing NG fraction, the smoke value drops sharply, as the gas is less carbon-rich and produces less smoke when burned. While the model offers somewhat more cautious, higher values, actual data reveal that smoke can fall around 2 m^{-1} and even below; the variation is not significant. The ANCOVA forecasts so properly show the developing pattern of smoke value decline, therefore verifying that more natural gas in engine running lowers soot emissions.

Figure 6a shows the values of the rate of combustion heat release (ROHR, J/°CA) from twelve experiments (blue curve) and the analogous values predicted by the ANCOVA model (red curve). Three engine loads (runs 1–4, 5–8 and 9–12) were selected for the tests, each of which varied the natural gas energy ratio from 0% to 80%. In the first interval (runs 1–4), at relatively low load, the observed ROHR values initially reach ~26–27 J/°CA and decrease towards 18–19 J/°CA as the NG fraction increases. The model curve also shows a clear decline, but initially tends to overestimate the real heat release rate (e.g., in run 2 the ANCOVA model fixes ~33.5 J/°CA, while the observed value is ~25.7). However, both directions of the curve coincide: intensive combustion without gas addition leads to a higher ROHR, and when the gas content increases to 80%, the release intensity drops noticeably. In the second interval (5–8 tests), when the load is medium, the experimental data show ROHR fluctuations from ~32 to 25–28 J/°CA, while the ANCOVA predictions are in a similar range (~31–25). Although at some points (e.g., 6–7 tests) the model again predicts slightly higher values, the overall gradual decrease – with increasing NG energy ratio –is clearly reflected in both the actual and model curves. In the third interval (9–12 tests), corresponding to the highest load (~90 kW), the observed ROHR values initially increase to 41–42 J/°CA, and then increase further (up to ~52 J/°CA). Meanwhile, the model curve in runs 9–10 has an overestimation (e.g., shows ~46.1 vs. 41.7), but in the last run (No. 12) – on the contrary, slightly underestimates the real value (~44 vs. 52.4). These changes indicate that at extreme loads, other factors, such as fuel injection strategy or chamber temperature distribution, can distort ANCOVA predictions more, since the model relies more on the general correlation between load, NG fraction and combustion acoustic variables. Despite several larger deviations, both data sets confirm the essential trend: a lower NG energy ratio leads to a sharper and more intense combustion (higher ROHR), and an increase in NG stretches the combustion process, reducing the instantaneous heat release rate. In addition, a higher load promotes an overall increase in ROHR, but the exact extent of the increase is not always perfectly predicted by the model. Thus, this comparison shows that the ANCOVA method generally correctly captures the main patterns, but in larger ROHR ranges (especially at high load), additional factors that may cause a greater discrepancy between actual and predicted values should be more carefully evaluated.

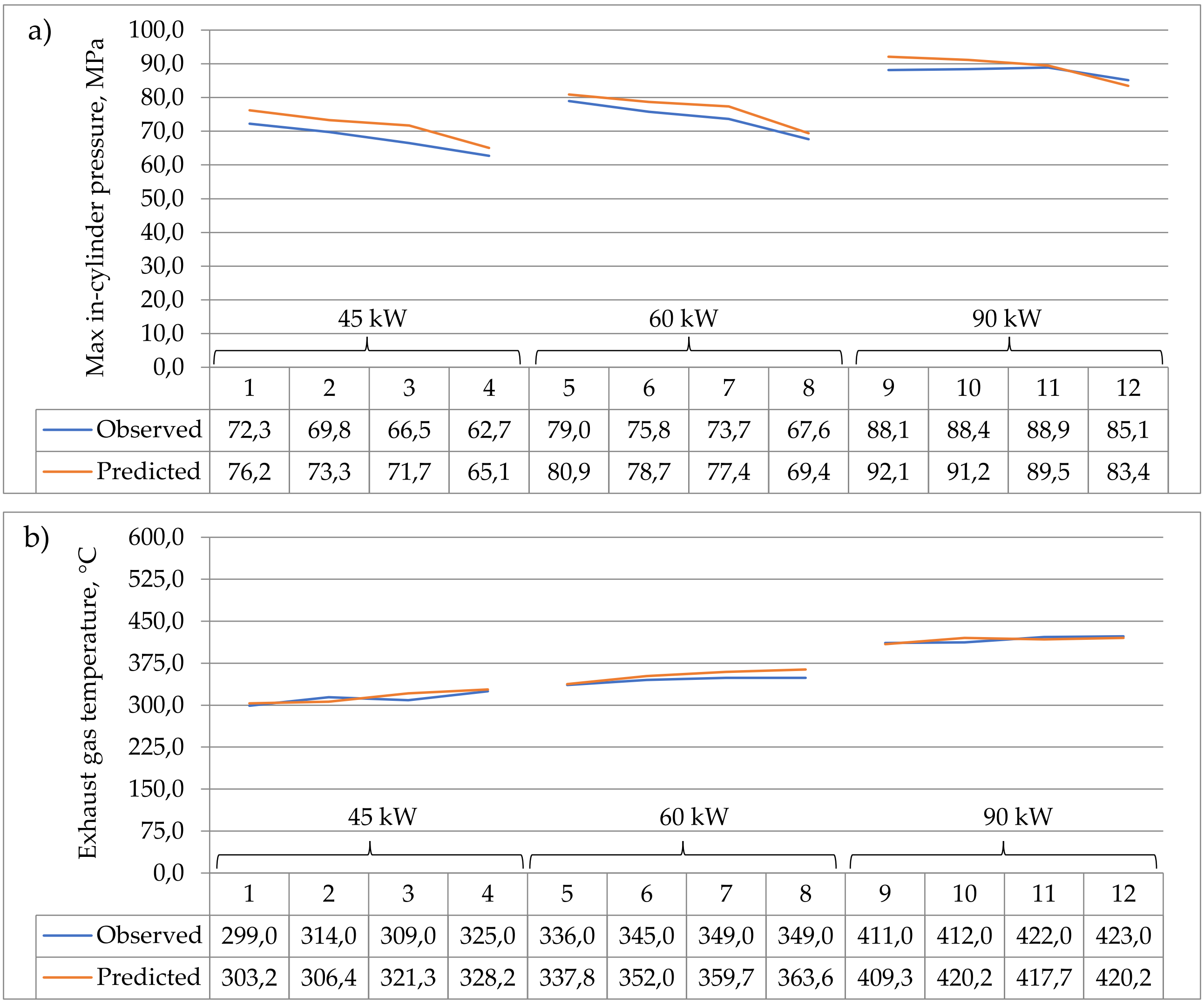

	1	2	3	4	5	6	7	8	9	10	11	12
Observed	72,3	69,8	66,5	62,7	79,0	75,8	73,7	67,6	88,1	88,4	88,9	85,1
Predicted	76,2	73,3	71,7	65,1	80,9	78,7	77,4	69,4	92,1	91,2	89,5	83,4

	1	2	3	4	5	6	7	8	9	10	11	12
Observed	299,0	314,0	309,0	325,0	336,0	345,0	349,0	349,0	411,0	412,0	422,0	423,0
Predicted	303,2	306,4	321,3	328,2	337,8	352,0	359,7	363,6	409,3	420,2	417,7	420,2

Figure 4. Measured engine operating cycle parameters real and prognostic values. Experiments 1-4, 5-8, and 9-12 include engine power of 45 kW, 60 kW, and 90kW, respectively. In each experiment block of unique engine power gas ratio are sorted in ascending order, i.e., experiment no. 1, 2, 3, and 4 includes gas ratio of of 0%, 40%, 60%, and 80%, respectively

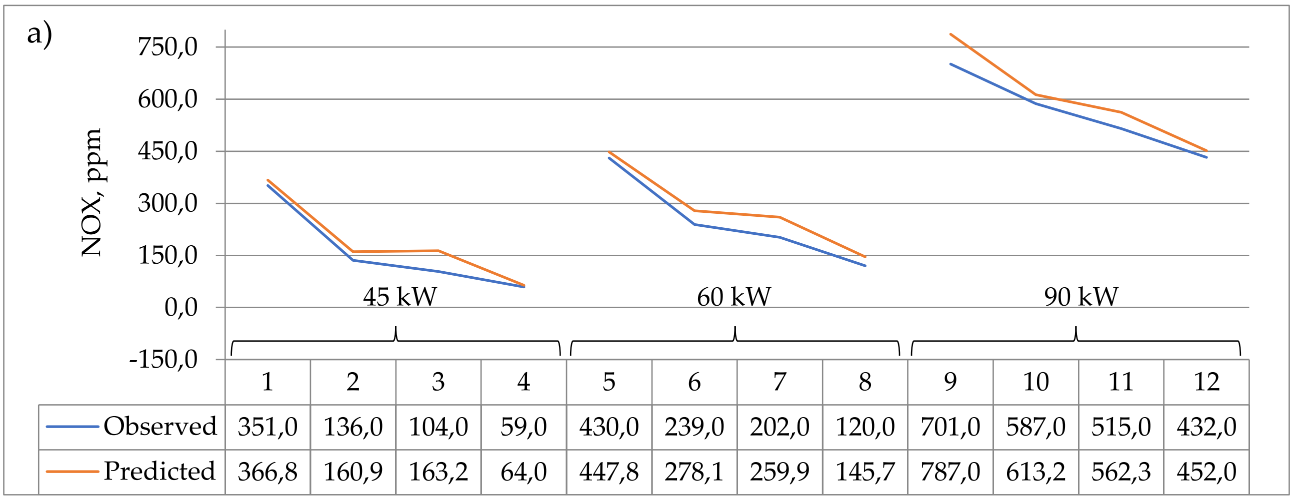

	1	2	3	4	5	6	7	8	9	10	11	12
Observed	351,0	136,0	104,0	59,0	430,0	239,0	202,0	120,0	701,0	587,0	515,0	432,0
Predicted	366,8	160,9	163,2	64,0	447,8	278,1	259,9	145,7	787,0	613,2	562,3	452,0

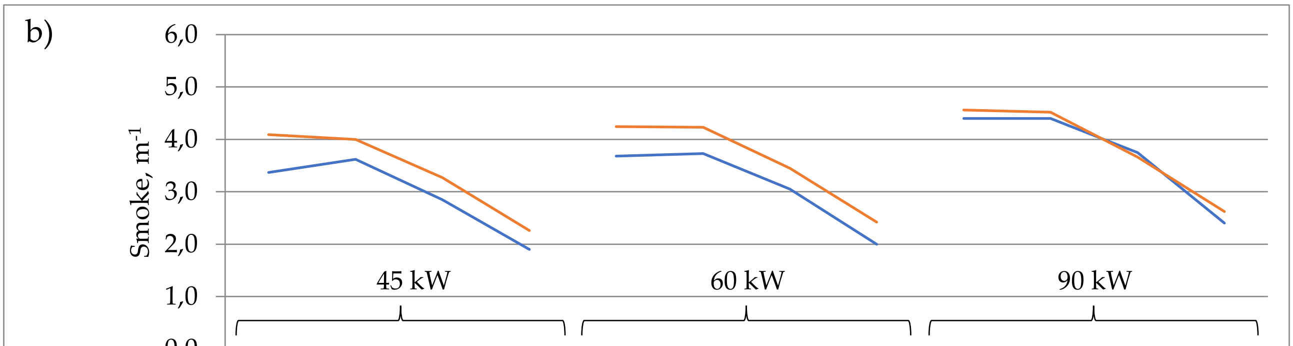

	1	2	3	4	5	6	7	8	9	10	11	12
Observed	3,4	3,6	2,9	1,9	3,7	3,7	3,1	2,0	4,4	4,4	3,8	2,4
Predicted	4,1	4,0	3,3	2,3	4,2	4,2	3,4	2,4	4,6	4,5	3,7	2,6

Figure 5. Measured engine emission parameters real and prognostic values. Experiments 1-4, 5-8, and 9-12 include engine power of 45 kW, 60 kW, and 90kW, respectively. In each experiment block of unique engine power gas ratio are sorted in ascending order, i.e., experiment no. 1, 2, 3, and 4 includes gas ratio of of 0%, 40%, 60%, and 80%, respectively

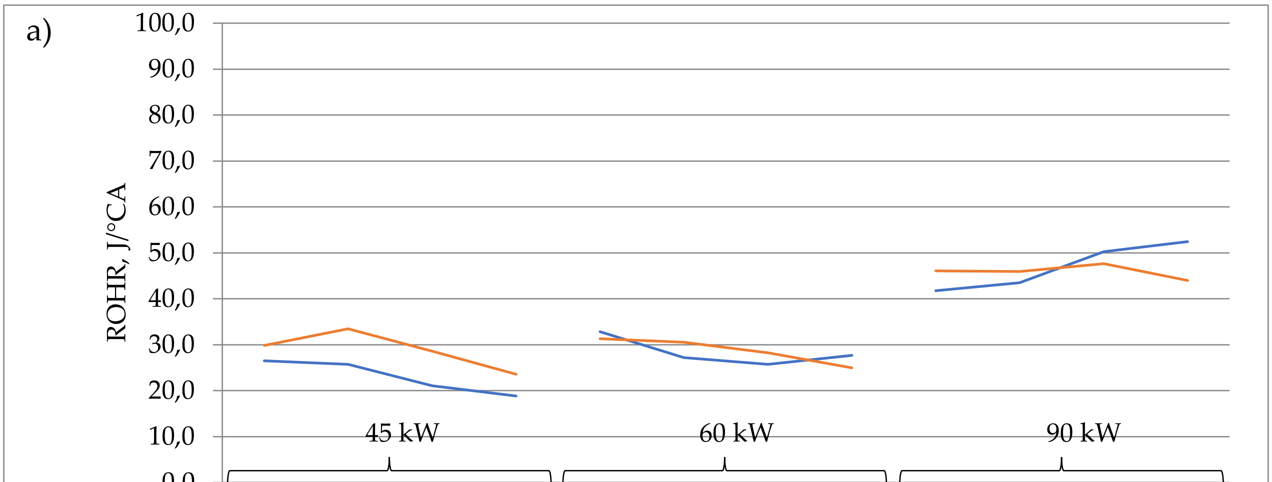

	1	2	3	4	5	6	7	8	9	10	11	12
Observed	26,5	25,7	21,0	18,8	32,8	27,2	25,7	27,7	41,7	43,5	50,3	52,4
Predicted	29,8	33,5	28,6	23,6	31,3	30,5	28,3	24,9	46,1	45,9	47,6	44,0

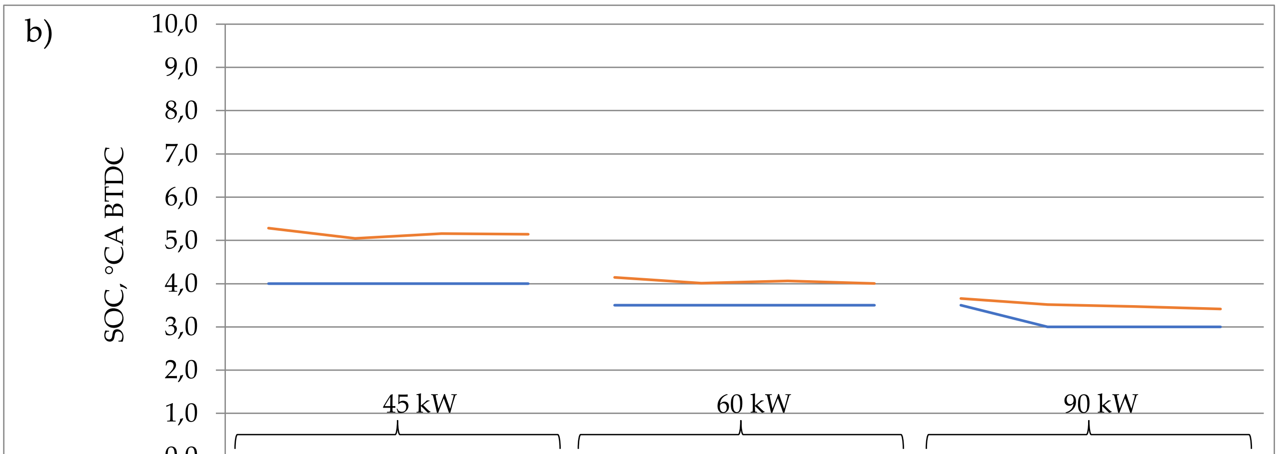

	1	2	3	4	5	6	7	8	9	10	11	12
Observed	4,0	4,0	4,0	4,0	3,5	3,5	3,5	3,5	3,5	3,0	3,0	3,0
Predicted	5,3	5,0	5,2	5,1	4,1	4,0	4,1	4,0	3,7	3,5	3,5	3,4

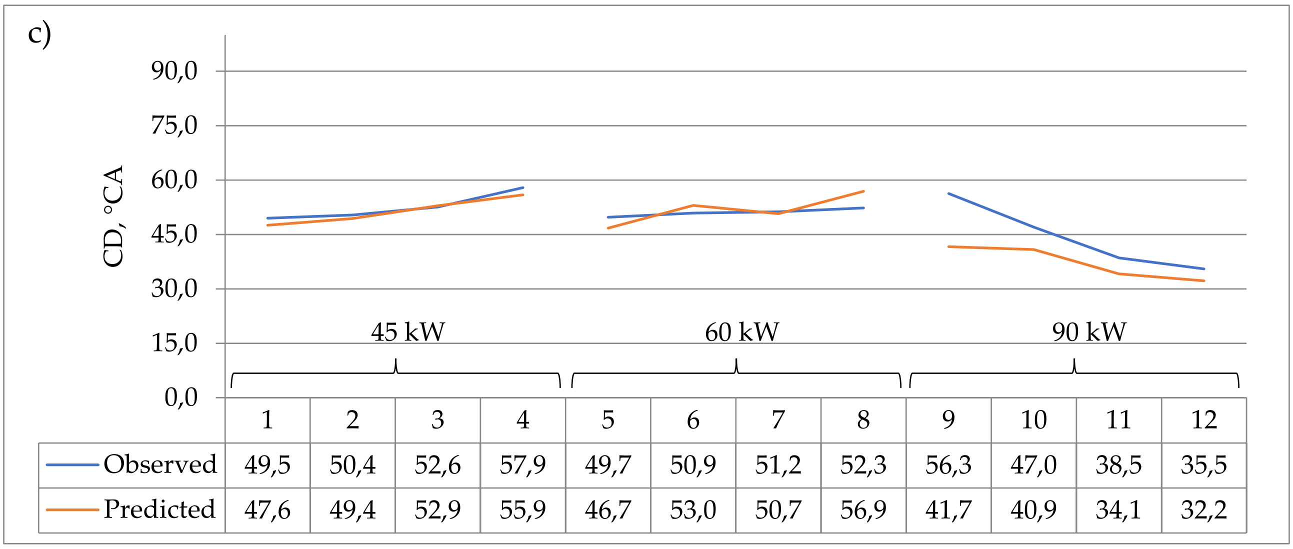

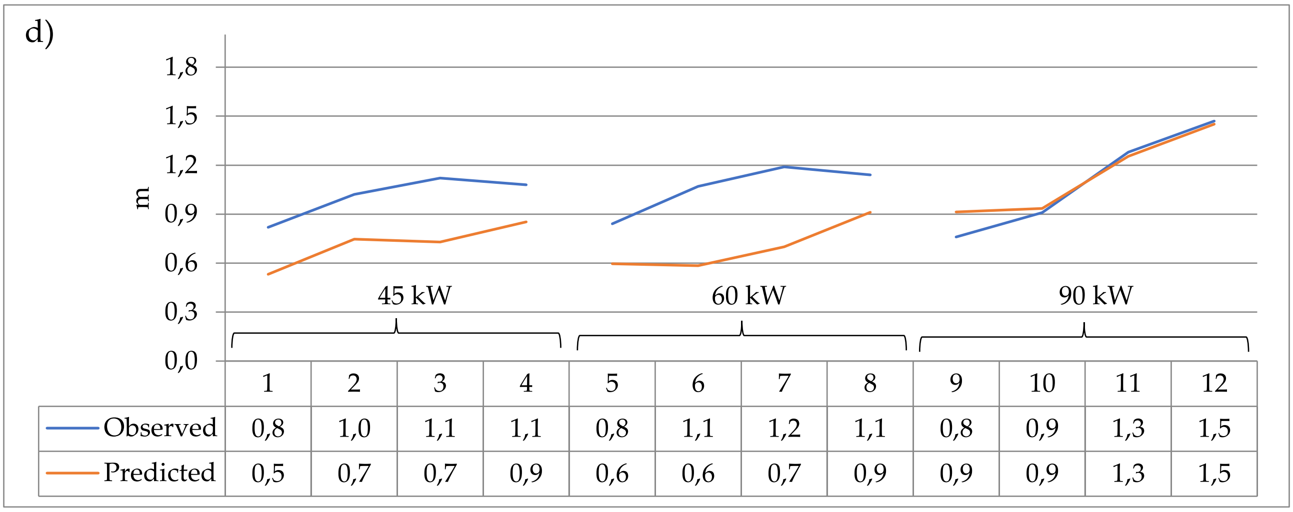

Figure 6. Measured engine combustion parameters real and prognostic values. Experiments 1-4, 5-8, and 9-12 include engine power of 45 kW, 60 kW, and 90kW, respectively. In each experiment block of unique engine power gas ratio are sorted in ascending order, i.e., experiment no. 1, 2, 3, and 4 includes gas ratio of of 0%, 40%, 60%, and 80%, respectively.

Figure 6b shows the variation of the start of combustion (SOC) timing parameter in CA degrees before top dead center (BTDC) in twelve tests (blue curve) and the value of the same parameter calculated by the ANCOVA model (red curve). It is obvious that there is a 1–2 °CA difference between the observed and predicted values, since the model line is higher in almost all tests. However, the overall dynamics of the curves in each experimental block (1–4, 5–8, 9–12) is essentially consistent: a higher value at the beginning gradually decreases when the NG energy ratio or the fuel mass is increased. In tests 1–4 (lowest load), the observed SOC timing values remain constant at 4.0 °CA, while the model predicts slightly higher values (5.0–5.3 °CA). This may be because the actual SOC timing changes less in this mode, and the model, due to the generally collated data, is more responsive to acoustic or vibrational variations. In tests 5–8, where the load is higher, both the actual and predicted values begin to decrease to ~3.5–4.1 °CA. In the highest load zone (tests 9–12), the observed SOC values drop to 3.0 °CA, while the model still shows 3.4–3.7 °CA. Although the ANCOVA curve systematically fixes a higher SOC timing value, the general trends coincide: with increasing engine power and changing fuel composition, the SOC value gradually shifts towards lower values. The final experiments (10–12) show that the SOC timing can decrease more sharply than the model predicts, but the overall magnitude of the decrease from ~4–5 to ~3 °CA is recorded in both curves. Such a consistent, ~1 °CA deviation between the model and the actual data set indicates that ANCOVA may tend to consistently override some of the ignition delay. However, given that the SOC timing is in reality very sensitive to fuel properties and temperature and dynamic changes in the engine, this deviation is not large and does not prevent the determination of general ignition course regularities.

Figure 6c shows the combustion duration (CD, °CA) values of twelve experimental runs (blue curve) and the prediction of the same data by the ANCOVA model (red curve). All runs are divided into three groups (1–4, 5–8 and 9–12), corresponding to increasing engine loads and different NG energy ratio. In the first group (runs 1–4), where the load is the lowest, the observed combustion durations start from about 49–50 °CA and increase to almost 58 °CA, when the NG energy ratio reaches 80%. This prolongation is associated with a milder combustion process, when part of the energy is supplied by gas. The ANCOVA model captures a similar trend (about 47.6 → 55.9 °CA), but in the fourth run it lags somewhat behind the real value (~58 vs. 56 °CA). In the second group (tests 5–8), at medium load, the CD varies between 49.7° and 52.3° CA degrees, while the model predicts a similar range (46.7° → 56.9°), sometimes overestimating the actual measurements (e.g., in test 8). However, the direction of change of both curves remains common: the combustion duration tends to increase with increasing gas fraction. In the third group (tests 9–12), at high load, the actual CD initially reaches 56 °CA, but in subsequent tests decreases to about 35–36 °CA. The model also shows a decreasing direction, although at some points (e.g., tests 9–10) it underestimates the observed duration significantly more. This indicates that in the most extreme regimes, some factors (e.g., temperature, pilot injection characteristics) have a greater influence on the combustion process than the general covariance model predicts. Overall, ANCOVA is quite successful in reproducing the regularities of the combustion duration variation when the engine load and the natural gas energy ratio change. At lower loads, combustion usually lengthens as the gas amount increases, while at the highest load, the combustion duration is initially long, but becomes significantly shorter as the NG energy ratio increases. Although in some tests, more significant deviations between the actual and model values are observed, their direction remains the same, allowing a reliable conclusion to be drawn about the influence of these factors on the combustion process.

Figure 6d shows the dynamics of the Wiebe equation factor m in twelve tests, where the blue curve represents the empirically measured values, and the red curve represents the ANCOVA model predictions. The tests are divided into three blocks (1–4, 5–8, 9–12), reflecting increasing engine load and different NG energy ratio. A high m value indicates a more even combustion, where more heat is released in the second part of the combustion, while a lower value indicates a concentrated and sharp combustion process just after SOC. In the first tests (1–4), at low load, the observed m values gradually increase from ~0.8 to ~1.1, indicating that the combustion becomes milder with increasing NG energy ratio. The ANCOVA model simultaneously provides lower predictions (0.5–0.9), but follows the same increasing trend, although it underestimates some of the combustion dispersion. The average load (5–8 trials) is characterized by a rise in m from ~0.8 to 1.2 (in trials 6–7) and a slight decline to ~1.1 (in trial 8). ANCOVA also predicts a rise, but at many points (especially at trial 7) it lags behind the actual peak. However, both data sets show the same rise–fall pattern: naturally, the influence of NG on the combustion process is less predictable here than at higher loads. In the maximum load interval (9–12 trials), the m values rise from ~0.8–0.9 to as much as 1.4–1.5. Here, the model predictions largely coincide with the actual values, reflecting an extremely good covariate relationship between the load, NG energy ratio, acoustic parameters, and combustion duration characteristics. Such a successful prediction shows that at high load the combustion process becomes more predictable, and a higher NG energy ratio provides more graduality (increased m). In summary, although in the first eight tests the ANCOVA model sometimes underestimates the observed m values, the general trend of increase or decrease coincides with the experimental data. Meanwhile, at high load (9–12 tests) both sets of curves overlap almost perfectly. From this it can be concluded that the Wiebe factor m reliably varies with the combination of natural gas fraction and load, and the constructed statistical model successfully reproduces the degree of stretching of the combustion process, especially at higher engine powers.

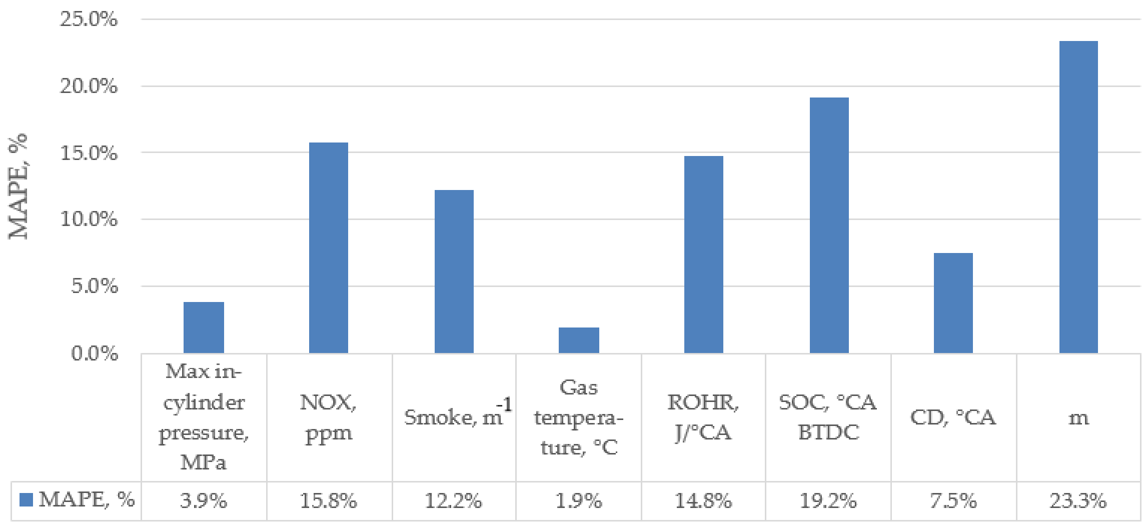

Figure 7. Mean absolute percentage error for engine outcome parameters calculated from prognostic ANCOVA model.

Figure 7 shows the mean absolute percentage errors (MAPE) for each of the engine parameters predicted by the ANCOVA model. MAPE indicates how much, on average (in percent), the model's predicted values deviate from the experimentally measured values, and therefore clearly shows which parameters are more accurately predicted and which are more difficult to predict.

The lowest errors (1.9%) were achieved when predicting exhaust gas temperature, indicating that the combustion heat balance and its dependence on load and NG energy ratio are of a fairly linear nature and are well captured by the statistical model. A relatively small MAPE (3.9%) is also observed for maximum pressure, indicating that the peak pressure dynamics characteristic of the combustion chamber successfully correlates with the variables included in the model.

The average accuracy can be attributed to the combustion duration (CD, 7.5%), which, although it has a more complex relationship with the combustion process, is still partially predictable according to the load and fuel composition. The smoke and NO_X emisions have a slightly higher error (12.2–15.8%), because the emission parameters are more influenced by the subtle nuances of the combustion processes (temperatures, excess oxygen, formation of the reaction zone), which are simply not described by the main ANCOVA factors.

The largest MAPEs (14.8–23.3%) are associated with the rate of combustion heat release (RORH), the SOC timing and the Wiebe equation factor m. These three indicators emphasize the onset, speed and degree of dispersion of combustion, and therefore are particularly sensitive to instantaneous changes in spray, mixture formation and temperature distribution in the engine. The load, NG energy ratio or basic acoustic parameters alone are not sufficient to describe them ideally, so the error remains more significant.

In summary, the lowest MAPE (1.9%) is achieved for temperature, and the highest (~23.3%) – for the combustion process parameter m. However, the error of most predictions does not reach 20%, indicating that ANCOVA predicts quite well the changes in engine performance and emissions when changing the load and HVO or diesel and NG energy proportions. Thus, the model confirms a more reliable prediction of macroscopic quantities (temperature, maximum in-cylinder pressure) and a worse reproduction of combustion process subtleties (SOC, RORH, Wiebe m).

MAPE analysis showed that the developed predictive model is sufficiently accurate, and the chosen methodology for its development is appropriate and reasonable. The accuracy of the model would improve if more data were used during model training. Of course, in order to firmly prove the universality of the model, more independent experiments using different fuels, engines, etc. should be performed.

4. Conclusions

1. Experimental results show that increasing the energy ratio of NG in a dual-fuel engine significantly reduces harmful emissions. As the NG energy ratio increases, maximum in-cylinder pressure, NO_X and smoke are significantly reduced, confirming that partial gas combustion softens the sudden rise in pressure and

lower combustion temperature limits the formation of nitrogen oxides. Smoke emissions are reduced due to the lower carbon to hydrogen ratio in NG and the longer combustion duration.

2. Replacing conventional diesel with hydrotreated vegetable oil (HVO) has been shown to significantly shorten the ignition delay. Although using pure HVO the level of vertical engine vibrations increases slightly, the HVO combustion process is cleaner, and when combined with NG, it allows reducing exhaust emissions without compromising engine performance.
3. Measured indicators such as maximum in-cylinder pressure, start of combustion, combustion duration show that the increasing NG energy ratio stretches combustion, reduces sudden pressure surges. Although the overall sound pressure level does not change significantly, frequency analysis shows that the sharpest impact frequencies are weakened, making the engine acoustics smoother.
4. The developed ANCOVA-based prediction model explains from 90% to 99% of the variations in the main parameters (peak in-cylinder pressure, NO_X, smoke, combustion duration, etc.). The mean absolute percentage error (MAPE) ranges from ~2% (exhaust gas temperature) to ~23% (Wiebe equation factor m). Macroscopic values (temperature, peak in-cylinder pressure) are reproduced quite accurately, but more complex combustion parameters (start of combustion, combustion heat release rate, m) require more detailed analysis.
5. Lower smoke emissions and lower peak temperature values with increasing NG energy ratio can reduce deposit accumulation and thermal load on components, resulting in longer engine maintenance intervals. Improved HVO characteristics—such as low sulfur content—can help to lower injector fouling even more and prolong the operating life of exhaust gas treatment systems. This helps to improve engine dependability, particularly in prolonged or high load operation.
6. Combining HVO and natural gas seems to be a good strategy to keep reasonable engine performance while reducing NO_X and smokiness. The proposed ANCOVA model provides a fast and cost-effective way to predict engine behavior when changing load and fuel mixture composition, and can be a valuable tool for engine improvement. In the future, it is appropriate to investigate more advanced injector control strategies, detailed cylinder temperature measurements, or the use of chemikine models, in order to more accurately reflect complex combustion processes at high loads and evaluate long-term changes in component reliability. In addition to performance and emission modeling, the ANCOVA approach also indirectly reflects factors that influence component longevity—such as dynamic loading and acoustic excitation—providing a useful foundation for future integration of predictive maintenance tools in dual-fuel engine systems.

Acknowledgements

This research was supported by the center of excellence project "Civil Engineering Research Center" (Grant No. S-A-UEI-23-5).

References

1. Adamiak B, Andrych-Zalewska M, Merkisz J, Chłopek Z. The uniqueness of pollutant emission and fuel consumption test results for road vehicles tested on a chassis dynamometer. Eksploatacja i Niezawodność – Maintenance and Reliability 2024. doi:10.17531/ein/195747, https://doi.org/10.17531/ein/195747.
2. Alahmer H, Alahmer A, Alkhazaleh R, Al-Amayreh M I. Modeling, polynomial regression, and artificial bee colony optimization of SI engine performance improvement powered by acetone–gasoline fuel blends. Energy Reports 2023; 9: 55–64, https://doi.org/10.1016/j.egyr.2022.12.102.
3. Borucka A, Wiśniowski P, Mazurkiewicz D, Świderski A. Laboratory measurements of vehicle exhaust emissions in conditions reproducing real traffic. Measurement 2021; 174: 108998, https://doi.org/10.1016/j.measurement.2021.108998.
4. Cohen J, Cohen J. Applied multiple regression/correlation analysis for the behavioral sciences. Mahwah, N.J., L. Erlbaum Associates:

2003.
5. da Costa R B R, Roque L F A, de Souza T A Z et al. Experimental assessment of renewable diesel fuels (HVO/Farnesane) and bioethanol on dual-fuel mode. Energy Conversion and Management 2022; 258: 115554, https://doi.org/10.1016/j.enconman.2022.115554.
6. Faizollahzadeh Ardabili S, Najafi B, Aghbashlo M et al. Performance and emission analysis of a dual-fuel engine operating on high natural gas substitution rates ignited by aqueous carbon nanoparticles-laden diesel/biodiesel emulsions. Fuel 2021; 294: 120246, https://doi.org/10.1016/j.fuel.2021.120246.
7. García A, Monsalve-Serrano J, Marco-Gimeno J, Iñiguez E. Data-driven modeling for predicting the steady-state and transient performance of a dual-fuel medium-duty engine employing artificial neural networks. Fuel 2025; 394: 135150, https://doi.org/10.1016/j.fuel.2025.135150.
8. García A, Monsalve-Serrano J, Marco-Gimeno J, Iñiguez E. Experimental evaluation of the optimal turbocharger system for a multi-cylinder dual-fuel engine towards the operation in transient conditions. Fuel 2025; 394: 135151, https://doi.org/10.1016/j.fuel.2025.135151.
9. Hai T, Hussein Kadir D, Ghanbari A. Modeling the emission characteristics of the hydrogen-enriched natural gas engines by multi-output least-squares support vector regression: Comprehensive statistical and operating analyses. Energy 2023; 276: 127515, https://doi.org/10.1016/j.energy.2023.127515.
10. Johnson S L, Clarke A, Fletcher T, Hylands D. A Phenomenological Approach to Dual Fuel Combustion Modelling. American Society of Mechanical Engineers Digital Collection: 2013: 781–791, https://doi.org/10.1115/ICEF2012-92133.
11. Kruczyński S, Ślęzak M. A simulation and experimental verification of the operation of the oxidising catalytic converter in diesel engine. Eksploatacja i Niezawodność – Maintenance and Reliability 2024. doi:10.17531/ein/184090, https://doi.org/10.17531/ein/184090.
12. Li T, Zhao P, He H et al. Dual-fuel dual-direct injection: An efficient and clean combustion technology for diesel engines. Journal of the Energy Institute 2025; 119: 102006, https://doi.org/10.1016/j.joei.2025.102006.
13. Mateus M M, Bordado J M, Galhano dos Santos R. Simplified multiple linear regression models for the estimation of heating values of refuse derived fuels. Fuel 2021; 294: 120541, https://doi.org/10.1016/j.fuel.2021.120541.
14. Matijošius J, Rimkus A, Gruodis A. Validation Challenges in Data for Different Diesel Engine Performance Regimes Utilising HVO Fuel: A Study on the Application of Artificial Neural Networks for Emissions Prediction. Machines 2024; 12(4): 279, https://doi.org/10.3390/machines12040279.
15. Milojević S, Stopka O, Kontrec N et al. Analytical Characterization of Thermal Efficiency and Emissions from a Diesel Engine Using Diesel and Biodiesel and Its Significance for Logistics Management. Processes 2025; 13(7): 2124, https://doi.org/10.3390/pr13072124.
16. Nguyen V G, Dager B, Chhillar A et al. Desirability-based optimization of dual-fuel diesel engine using acetylene as an alternative fuel. Case Studies in Thermal Engineering 2024; 59: 104488, https://doi.org/10.1016/j.csite.2024.104488.
17. Peng Y, Hai W, Xue P. Fault diagnosis analysis of gas turbine engine based on fuzzy algorithm. Diagnostyka 2025; 26(1): 1–13, https://doi.org/10.29354/diag/200870.
18. Pinto G M, da Costa R B R, de Souza T A Z et al. Experimental investigation of performance and emissions of a CI engine operating with HVO and farnesane in dual-fuel mode with natural gas and biogas. Energy 2023; 277: 127648, https://doi.org/10.1016/j.energy.2023.127648.
19. Pinto G M, de Souza T A Z, da Costa R B R et al. Combustion, performance and emission analyses of a CI engine operating with renewable diesel fuels (HVO/FARNESANE) under dual-fuel mode through hydrogen port injection. International Journal of Hydrogen Energy 2023; 48(51): 19713–19732, https://doi.org/10.1016/j.ijhydene.2023.02.020.
20. Rimkus A, Žaglinskis J, Stravinskas S et al. Research on the Combustion, Energy and Emission Parameters of Various Concentration Blends of Hydrotreated Vegetable Oil Biofuel and Diesel Fuel in a Compression-Ignition Engine. Energies 2019; 12(15): 2978, https://doi.org/10.3390/en12152978.
21. Sabzehali M, Alibeigi M, Aliabadi S K. Low-emission methane fueled dual-bypass turbofan engine optimization based on machine learning: Energy-economic-environmental (3E) analysis. Cleaner Engineering and Technology 2025; 26: 100919, https://doi.org/10.1016/j.clet.2025.100919.
22. Selech J, Matijošius J, Kilikevičius A, Marinkovic D. Reliability Analysis and the Costs of Corrective Maintenance for a Component of a Fleet of Trams. Tehnicki vjesnik - Technical Gazette 2025. doi:10.17559/TV-20241121002144, https://doi.org/10.17559/TV-

20241121002144.
23. Sharma P, Sahoo B B. Precise prediction of performance and emission of a waste derived Biogas–Biodiesel powered Dual–Fuel engine using modern ensemble Boosted regression Tree: A critique to Artificial neural network. Fuel 2022; 321: 124131, https://doi.org/10.1016/j.fuel.2022.124131.
24. Sharma P, Sahoo B B, Said Z et al. Application of machine learning and Box-Behnken design in optimizing engine characteristics operated with a dual-fuel mode of algal biodiesel and waste-derived biogas. International Journal of Hydrogen Energy 2023; 48(18): 6738–6760, https://doi.org/10.1016/j.ijhydene.2022.04.152.
25. Sun W, Wang X, Guo L et al. Study on effects of EGR and injection strategies on the combustion and emission characteristics of ammonia/diesel dual-fuel engine. Energy 2025; 315: 134391, https://doi.org/10.1016/j.energy.2025.134391.
26. Szabados G, Knaup J, Bereczky Á. ICE Relevant Physical-chemical Properties and Air Pollutant Emission of Renewable Transport Fuels from Different Generations – An Overview. Periodica Polytechnica Transportation Engineering 2022; 50(1): 11–22, https://doi.org/10.3311/PPtr.14925.
27. Tarabet L, Loubar K, Lounici M S et al. Experimental investigation of DI diesel engine operating with eucalyptus biodiesel/natural gas under dual fuel mode. Fuel 2014; 133: 129–138, https://doi.org/10.1016/j.fuel.2014.05.008.
28. Uluocak I, Uludamar E. Comparative evaluation of machine learning models for predicting noise and vibration of a biodiesel-CNG fuelled diesel engine. Measurement 2025; 249: 117021, https://doi.org/10.1016/j.measurement.2025.117021.
29. Wan Mahdi W N I, Ithnin A M, Yahya W J et al. A comparative review of alternative fuels: Diesel-HHO and diesel-hydrogen via enrichment method in diesel engines application. International Journal of Hydrogen Energy 2025; 120: 444–472, https://doi.org/10.1016/j.ijhydene.2025.03.319.
30. Zhou F, Liu N, Zhang X, You X. 1D study of the detonation phenomenon and its influence on the interior ballistics of the combustion light gas gun. Defence Technology 2019: S2214914719303253, https://doi.org/10.1016/j.dt.2019.06.009.
31. Žvirblis T, Hunicz J, Matijošius J et al. Improving Diesel Engine Reliability Using an Optimal Prognostic Model to Predict Diesel Engine Emissions and Performance Using Pure Diesel and Hydrogenated Vegetable Oil. Eksploatacja i Niezawodność – Maintenance and Reliability 2023. doi:10.17531/ein/174358, https://doi.org/10.17531/ein/174358.
32. Žvirblis T, Vainorius D, Matijošius J et al. Engine Vibration Data Increases Prognosis Accuracy on Emission Loads: A Novel Statistical Regressions Algorithm Approach for Vibration Analysis in Time Domain. Symmetry 2021; 13(7): 1234, https://doi.org/10.3390/sym13071234.

Nomenclature	
ABC	Artificial Bees Colony Algorithm
AC10	Gasoline fuel and 10 % of acetone by volume fuel mixture
ANCOVA	Analysis of covariance
ANN	Artificial neural network
BRT	Boosted regression trees
BTE	Brake thermal efficiency
CA	Crankshaft rotation angle
CD	Combustion duration
CH_4	Methane
CI	Compression ignition
CO	Carbon monoxide
CO_2	Carbon dioxide
EGR	exhaust gas recirculation
HC	Hydrocarbon
HVO	Hydrotreated vegetable oil
IC	Internal combustion
LHV	Lower heating values
M_B	Engine load torque
MAPE	Mean absolute percentage error

ML	Machine learning
MLS-SVR	Least-squares support vector regression
NG	Natural gas
RMSE	Root mean square error
NO_X	Nitrogen oxide
O_2	Oxygen
R^2	Coefficient of determination
RMS	Root mean square
ROHR	Rate of heat release
SD	Standard deviation
SI	Spark ignition
SOC	Start of combustion